MJFAS
Malaysian Journal of Fundamental and Applied Sciences

Mogan *et al.* | Malaysian Journal of Fundamental and Applied Sciences, Vol. 22 (2026) 670-689

RESEARCH ARTICLE

Fabrication and Optimisation of Alginate/Agarose Silver Nanocomposites Hydrogel Towards Antimicrobial Activities

Veithesswary Mogan[a], Norshamiza Abu Bakar[a] ,Dr. Norhayati Yusop[a], Dr. Juan Matmin[b], Dr. Nur Fatiha Binti Ghazalli[a]*

[a]School of Dental Sciences, Universiti Sains Malaysia, Health Campus, 16150 Kubang Kerian, Kelantan, Malaysia; [b]Department of Chemistry, Faculty of Science, Universiti Teknologi Malaysia, 81310 UTM Johor Bahru, Johor, Malaysia.

Abstract The co-implantation of alginate (Al) and agarose (Ag) with silver nanoparticles (AgNPs) is one of the feasible strategies to develop nanocomposite hydrogels for future wound dressings. Natural hydrogels have emerged as promising materials because of their excellent biocompatibility; however, they experience poor mechanical strength and infection susceptibility. This study aims to 3synthesise and optimise AgNP-loaded alginate-agarose composite hydrogel beads and to comprehensively evaluate their physiochemical, mechanical, antimicrobial, and cell attachment performance for potential applications in wound dressing. Composite hydrogels were synthesised using alginate and agarose with different ratios and loaded with silver nanoparticles. Structural characterisation was carried out by Field emission scanning electron microscopy (FESEM) and transmission electron microscopy (TEM). Fourier transform infrared (FT-IR) spectroscopy was used to analyse the chemical interactions. The functional properties were analysed through swelling ratio measurement, mechanical strength (ASTM D638 Type V), and antibacterial assay *against Pseudomonas aeruginosa (P. aeruginosa), Staphylococcus aureus (S. aureus), and Escherichia coli (E. coli).* FESEM and TEM images revealed that the nanocomposite hydrogels have a porous structure and the AgNPs were well dispersed (6.6–22.9 nm, mean 14.1 nm). The FTIR data showed a strong coordination of silver ions with carboxylate groups in the polymer network. The swelling analysis also showed that the hydrogels are suitable for exudate management. The mechanical strength analysis of the $Al_{1.8}$–$Ag_{2.6}$ formulation brought the best compromise between strength (Young's modulus 20.7 kPa) and flexibility. Moreover, the antibacterial assay confirmed the excellent bactericidal effect against the tested bacteria. The optimised $Al_{1.8}$–$Ag_{2.6}$ nanocomposite hydrogel beads showed a synergistic improvement in mechanical strength, antimicrobial activity and cytocompatibility. This study demonstrates that AgNP-loaded alginate-agarose hydrogel has significant potential as an antimicrobial wound dressing materials.

Keywords: Alginate–agarose hydrogel, Silver nanoparticles, Nanocomposite wound dressing, Mechanical properties, Antibacterial activity.

***For correspondence:**
fatiha85@usm.my

Received: 04 December 2025
Accepted: 15 June 2026

Introduction

As a result of several decades of profound research effort in the field of biomedical materials science, a radical paradigm shift has emerged in recent times, with hydrogel being the most trendy biomaterial field of interest [1–3]. This enthusiasm has been stimulated by their sole manner of biomimicking physical, chemical, and biological characteristics of the native biological tissues [4]. Hydrogel is a term used to describe a hydrophilic, porous, three-dimensional polymeric network structure, with the ability to take up very large quantities of water or biological fluids [5-6]. Hydrogel is also biomimetic in biocompatibility due to its soft and pliable composition with a high content of water and non-adhesiveness [7]. All these

characteristics have directed hydrogel to be selected as a biomaterial in wound care, where a moist wound environment for wound healing is important to accelerate re-epithelialization, lessen scar formation and pain during dressing changes [8]. Furthermore, the scope to incorporate various bioactive compounds from drugs to cells and factors gives hydrogel the potential capability to be used not only as an inert dressing but also as a functional therapeutic system [9,10].

Although these are quite clearly advantageous, a single natural biopolymer normally does not provide the mechanical strength required for clinical applications [11]. Although materials such as alginate, collagen, and chitosan are cell-compatible, they are weak and not load-bearing or long-term structural capable materials [12,13]. For instance, the excellent biocompatibility of alginate is conventionally paid for with a poor structure, which cannot bear the physiological shear stress associated with a wound bed [14,15]. Likewise, for a material like agarose, it can provide the necessary stiffness via its thermal gelation, yet it is brittle and lacks cell-signalling domains and thus has limited utility on its own. In order to meet these market needs, the field has therefore moved towards composite systems [16,17]. The combination of several different types of polymers in one system allows us to create “synergistic” materials [18]. Alginate, a product of brown seaweed, is useful for its elasticity and ability to support the moist microenvironment associated with the treatment of high-exudate chronic wounds [19]. Agarose, on the other hand, has a structural architecture which is similar to the natural tissue structure and allows for the diffusion of oxygen and nutrients for a regenerative scaffold [20]. Through the combination of these two polymers, we are able to develop a composite with extracellular matrix (ECM)-like mechanical profile, and therefore a stronger scaffold for functional tissue repair.

Recently, in biomaterials science, there has arisen tremendous and increasing attention on developing nanocomposite hydrogels over conventional hydrogels for wide biomedical applications [21]. A nano-composite hydrogel referred to as a 3-D hybrid network is produced by loading nanoparticles into polymer chains. The addition of nanomaterials is a deliberate method to bring beneficial properties that are not present in the original hydrogel matrix, such as superior mechanical strength and electrical conductivity and antimicrobial activity [22]. AgNPs are one of the most investigated for their powerful antibacterial effect. Incorporated it into different synthetic and natural hydrogels to produce composite hydrogels for the decrease in bacterial infection in medicinal applications [23,24]. Microbial infection of chronic wounds is still an unprecedented menace. It can be attributed to the need for wound dressing with inherent antimicrobial properties to inhibit the development of biofilm or sepsis [25]. Recent reports indicate that biofilm development is a major cause of delays in wound healing in most chronic wounds. *Pseudomonas aeruginosa*, a typical pathogen that is commonly trapped and constrained by its sturdy matrix, has been at the core of the development of a biofilm no longer responsive to conventional antibiotics [26,27]. The addition of nanomaterials to cell-laden hydrogels enhances their physicochemical and biological properties. It is also a versatile approach toward the preparation of a versatile structure for tissue engineering [28,29].

The development of the nanocomposite hydrogel showed excellent properties and better processability than the hydrogel in optimal conditions. Moreover, the development of nanocomposite hydrogels also showed excellent photothermal conversion ability, which is a significant determining factor in their antibacterial action. This further confirms the advantages of nanocomposite hydrogels compared with hydrogel [30]. Accordingly, the present study aims to prepare a natural nanocomposite hydrogel with excellent mechanical and antibacterial properties as a biomaterial. This study aimed to systematically investigate the concentration of polymer components and precursors of silver to develop the best composition with optimum performance in terms of swelling ability, mechanical properties, and structure stabilization and antibacterial properties.

Although silver nanoparticle loaded hydrogels have been widely explored for wound healing, significant challenges still exist to achieve an optimum compromise in mechanical stability, swelling behavior, antimicrobial efficacy and cytocompatibility. Most reported studies have focused on either incorporation of AgNPs into pre-existing hydrogel matrices or evaluation of individual performance parameters. Moreover, the incorporation of AgNPs often leads to aggregation and non-uniform distribution, which can negatively impact biological performance. Hence, the novelty of our current study is to develop an alginate–agarose nanocomposite hydrogel using in-situ AgNP formation coupled with a systematically optimized formulation approach. By systematically correlating physicochemical properties, mechanical performance, swelling behavior, antimicrobial efficacy, and cellular compatibility, this study identified an optimized hydrogel formulation that balances multifunctional performance required for wound dressings. [31].

Materials and Methods

All chemicals used in this study were of analytical grade to maintain the experimental rigor and reproducibility. All reagents, including alginic acid sodium salt powder, Calcium chloride dihydrate $CaCl_2 \cdot 2H_2O$, Silver nitrate-ACS reagent (≥ 99.0%) and Sodium citrate tribasic dihydrate-ACS reagent (≥ 99.0%), $HO–C(COONa)(CH_2COONa) \cdot 2H_2O$, were obtained from Sigma-Aldrich. High-grade setting agarose, HyAgarose™ LE Multi-purpose Agarose was purchased from Hydragene. These choices were informed by the known purity and biomedical applicability of the materials, to isolate material properties as the variables of interest.

Synthesis of Alginate-Agarose (Al-Ag) composite

Three formulations were synthesised for comparative purposes. A control (1.5% alginate–2.3% agarose, hereafter referred to as $Al_{1.5}–Ag_{2.3}$) and two high-concentration formulations (1.8% alginate–2.6% agarose, $Al_{1.8}–Ag_{2.6}$ and 2.1% alginate–2.9% agarose, $Al_{2.1}–Ag_{2.9}$). To prepare the control formulation, 1.5% alginate stock solution was made by adding 1.5 g sodium alginate (Sigma-Aldrich) to 100 mL of distilled water. Simultaneously, 2.3 % agarose solution was prepared by adding 2.3 g of HyAgarose™ LE powder to 100 mL of distilled water. Agarose solution was heated to boiling point 98°C then cooled to 41°C. Then, the alginate solution was added, and the set mixture was kept at 41°C. A peristaltic pump fitted with an 18-G hypodermic needle, positioned 4 cm from a gelling bath consisting of 0.3 M calcium chloride, was used to dispense the blended solution to form solid beads. Synthesis was repeated for the $Al_{1.8}–Ag_{2.6}$ and $Al_{2.1}–Ag_{2.9}$ formulations.

Fourier Transform Infrared Spectroscopy analysis

Surface excess humidity was wiped away using sterile Kim. The sample was transferred immediately to an FTIR spectrometer with an Attenuated Total Reflectance (ATR) accessory for direct analysis of the hydrated polymer surfaces without extensive pretreatment. Spectra were recorded between wavenumber 4000–400 cm^{-1}, resolution 4 cm^{-1}.The ATR crystal was rinsed with ethanol in between samples. Spectral data were processed, baseline-corrected, and peaks were assigned using Sma4win (version 1.48) and ChemDraw Professional (version 22.0). The categorization of functional groups was carried out according to ASTM E1252-98 of infrared spectroscopy.

Field Emission Scanning Electron Microscopy

The investigations were carried out on the samples in their unmixed state without freeze-drying. The images of the samples were taken on the field emission scanning electron microscope in the low vacuum mode at an accelerating voltage of 5.0 kV. The images were taken at 500x to 20,000x magnifications to further elucidate the microstructures that were observed.

Degree of swelling ratio analysis

The initial weight of each hydrogel bead before incubation was measured. To calculate the swelling ratio, before incubation, the samples were oven-dried at 40°C for 24hrs until the dry weight (W_a). The dried beads were placed into 300 μL Gibco PBS solution at 37°C for different times (10, 20, 30, 40, 50, 60, 90, 120, 180, and 360 mins). After different time points, the beads were taken out, and gently picked with lint-free paper, then the weight (W_β.) of each bead was measured. The water uptake was calculated by following the equation: Degree of swelling (%) = $[(W_\beta – W_a) / W_a] \times 100\%$. All experiments were performed in triplicate and results are presented as mean ± standard deviation.

Tensile strength test

The mechanical tensile strength of all the alginate–agarose hydrogel formulations was tested by forming dumbbell-shaped specimens according to ASTM D638 Type V standard dimensions for consistent and comparable data. The samples were then air-dried in a universal oven at 30 °C for 6 hours. The tensile property assessment was carried out with a Shimadzu Universal Testing Machine (USA) equipped with a load cell of precision, in single mode. The samples were stretched at a crosshead speed of 1 mm/min without preload. The data was continuously measured and subsequently graphed as stress–strain equal to the force and displacement data, respectively, to obtain the ultimate tensile strength and elongation at break of the hydrogel formulations.

Preparation of silver nitrate solution

Silver nitrate was diluted in 3 different concentrations: 0.06 M (1.0 g), 0.09 M (1.5 g), and 0.12 M (2.0 g). The exact mass of silver nitrate (ACS reagent, ≥99.0%) was weighed for each formulation and dissolved in 100 mL of distilled water. The solution was heated up to an approximate temperature of 57.6°C and turned slightly pink. The heating process was stopped when the solution was close to boiling. The

procedure was repeated for all three concentrations.

UV-Visible spectrophotometry Analysis of Silver Nanoparticles

All the solutions were freshly prepared and equilibrated to room temperature before measurements to maintain similar conditions. The spectra were collected using a Shimadzu UV–Vis spectrophotometer (USA) with the instrument calibrated according to the manufacturer's guidance. The absorbance spectra were obtained between 300 and 700 nm with a 1 nm resolution. A baseline correction with deionised water as a reference was applied. Spectral acquisition was limited to the expected wavelength range of the surface plasmon resonance peaks, which is a distinctive peak for silver nanoparticles, ranging from 400–450 nm. Spectra were interpreted in terms of peak position, peak intensity, and peak bandwidth as these are correlated to the size distribution and the aggregate state.

Synthesis of Al-Ag composite incorporated with silver nanoparticles

Two sets of alginate–agarose beads were prepared with three different compositions, $Al_{1.5}$-$Ag_{2.3}$, $Al_{1.8}$-$Ag_{2.6}$ and $Al_{2.1}$-$Ag_{2.9}$. The first set of beads was immersed in characterized silver nitrate solutions (0.06 M, 0.09 M and 0.12 M) for 24 hrs. The second set was treated using a two-step method, first immersed in silver nitrate solution for 24 hrs and then immersed in 1% trisodium citrate solution for 24 hours. This allowed the study to compare the treated beads with and without a reducing agent. After the treatment was completed, all the beads were taken out and washed thoroughly with autoclaved distilled water. Hydrogel beads with varying concentrations of alginate and agarose, each incorporated with silver nanoparticles, were subjected to a multi-level characterisation process. This included Fourier Transform Infrared Spectroscopy (FTIR), Field Emission Scanning Electron Microscopy coupled with Energy Dispersive X-ray analysis (FESEM-EDX), Transmission Electron Microscopy (TEM), and swelling ratio analysis. These evaluations were performed to identify the optimal alginate–agarose nanocomposite concentration.

Antibacterial activity test

Three representative bacterial strains were tested to assess the antibacterial activity of alginate-agarose hydrogel integrated with silver nanoparticles. The strains included *E. coli*, a Gram-negative bacterium, *S. aureus*, a Gram-positive bacterium, and *P. aeruginosa*, also Gram-negative. Two antibacterial tests were conducted: total plate count and agar diffusion test, using an optimized $Al_{1.8}$–$Ag_{2.6}$ composite with silver nanoparticles and trisodium citrate. The hydrogel beads contained varying concentrations of silver nanoparticles; 0.06 M, 0.09 M and 0.12 M, designated as samples A (Al-Ag-1g), B (Al-Ag-1.5g), and C (Al-Ag-2g) respectively. A control sample, labelled as sample D, used pure alginate-agarose hydrogel, referred to as pure Al-Ag. The antibacterial efficacy was then determined using both total plate count and agar diffusion method. All experiments were performed in triplicate and results are presented as mean ± standard deviation.

Cell Attachment and Morphological Evaluation

Dental Pulp Stem Cells (DPSC) were cultured in α-minimum essential medium (α-MEM) supplemented with 10% fetal bovine serum (FBS) and 1% penicillin–streptomycin under standard incubation conditions (37°C, 5% CO_2, humidified atmosphere). Hydrogel samples ($Al_{1.8}$–$Ag_{2.6}$), including pristine and AgNP-loaded variants (0.06 M, 0.09 M, and 0.12 M), were prepared in sterile 6-well culture plates with a uniform thickness of approximately 1 cm. Prior to cell seeding, the hydrogel samples were sterilized and equilibrated in culture medium. DPSCs were then seeded onto the hydrogel surfaces and incubated for 48 hours. Following incubation, the samples were gently rinsed with phosphate-buffered saline (PBS). The adhered cells were subsequently fixed and subjected to freezing at −20°C for 72 hours, followed by freeze-drying for 48 hours to preserve cellular morphology. The dried samples were sputter-coated with a thin layer of gold and examined using field emission scanning electron microscopy (FESEM) at an accelerating voltage of 5 kV. Cell attachment, surface coverage, and morphological characteristics were analysed at magnifications ranging from 500x to 20,000x.

In Vitro Cytotoxicity Assay

Human Dermal Fibroblast cell lines (HDF) PCS-201-012 ™ was purchased from American Type Culture Collection (ATCC), USA. Cell lines were cultured in complete Dulbecco's Modified Eagle Medium (DMEM) supplemented with 10% fetal bovine serum (FBS) and 1% penicillin-streptomycin (1% pen-strep) at 37°C in a humidified 95% air and 5% CO_2 atmosphere. A preliminary Alamar Blue screening was conducted to optimise the silver loading in the hydrogel formulation. The initial lowest concentration of 0.06 M $AgNO_3$, showed reduced HDF cell viability. Therefore, the silver precursor concentration was reduced to 0.015M and this formulation was selected for further cytocompatibility evaluation. An extract-based method ISO 10993-12 with reference to ISO 10993-5 was used to prepare the extract of $Al_{1.8}$-$Ag_{2.6}$ nanocomposite beads. This method was slightly modified from earlier hydrogel cytocompatibility

studies. Briefly, 0.1g of sterile $Al_{1.8}$-$Ag_{2\ .6}$ nanocomposite beads containing 0.015 M AgNPs was immersed in 1 mL of complete DMEM and incubated at 37°C in a humidified 5% CO_2 incubator for 24 hours. The conditioned medium was then collected and filtered using a sterile 0.22 µm membrane filter. This undiluted conditioned medium was designated as the 100% hydrogel extract. Serial dilutions of the nanocomposite extract were prepared using complete DMEM to obtain 50%, 25%, 12.5%, and 6.25% extract concentrations. HDF cells were seeded into 96-well plates at 1 × 10^4 cells/well and incubated for 24 hours to allow cell attachment. The culture medium was then replaced with 100 µL of the respective conditioned medium and incubated for another 24 hours. Cells cultured in complete DMEM without hydrogel extract served as the untreated control and were considered as 100% viability.

Cell viability was determined using Alamar Blue reagent. Briefly, Alamar Blue was added at 10% (v/v) of the culture volume and incubated for 4 hours at 37°C. Fluorescence intensity was measured at 560 nm excitation and 590 nm emission using Thermoskan Lux multimode microplate reader. The percentage of cell viability was calculated relative to the untreated control. Statistical analysis of cell viability data was performed using repeated-measures one-way ANOVA followed by Tukey's post hoc test to determine significant differences between groups ($p<0.05$ considered statistically significant).

Results and Discussion

The present work clearly demonstrates that hybridization of agarose and alginate into a composite hydrogel improves structural stability and functional properties as compared with the individual single polymer systems. The hybridization overcomes the limitation of natural hydrogels, which is their typically very low tensile strength. The hybrid beads were significantly firmer and more mechanically robust compared to the individual alginate beads or agarose beads, a characteristic that is pivotal to many expected biomedical applications.

Macroscopic and Morphological Properties of Alginate–Agarose Composite Beads

The bead formation process was able to achieve an ideal spherical morphology. Visual and palpation tests showed that beads with higher percentages of each polymer were presumably more rigid and more difficult to deform. Hence, a higher percentage of polymer would impart a higher cross-linking density that would result in higher mechanical strength. The hydrogel exhibited a yellow hue, the intensity of which was directly correlated to the concentration of alginate in the matrix. This could be due to the natural colour of the alginate or the interaction of calcium ions with the alginate during the gelation process. The physical properties indicate that a successful interaction has occurred between the two biopolymers, with the agarose forming a rigid, tightly cross-linked skeleton around the more malleable alginate as can be seen in figure 1.

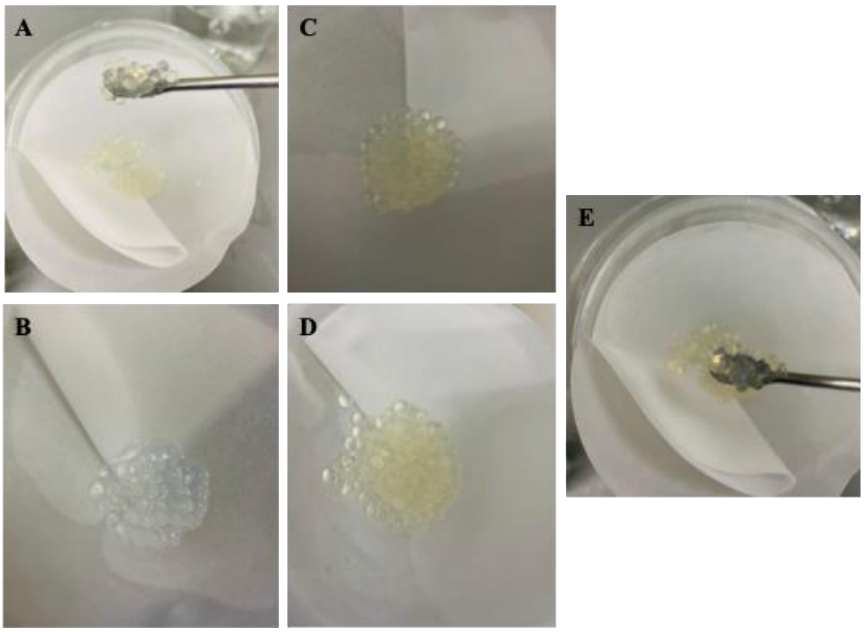

Figure 1. Morphological characteristics of alginate–agarose hydrogel beads. Panels showed (A) pure alginate and (B) pure agarose beads, alongside composite beads with progressively higher polymer concentrations: (C) $Al_{1.5}$–$Ag_{2.3}$, (D) $Al_{1.8}$–$Ag_{2.6}$, and (E) $Al_{2.1}$–$Ag_{2.9}$.

Physicochemical and Mechanical Characterisations of Alginate–Agarose Composite Beads

Mechanical testing (Table 1; Figure 2H) also demonstrated the expected increase in rigidity and strength with polymer concentration, with the lowest modulus being 15.2 kPa for $Al_{1.5}$–$Ag_{2.3}$, 20.7 kPa for $Al_{1.8}$–$Ag_{2.6}$, and 32.8 kPa for $Al_{2.1}$–$Ag_{2.9}$. For comparison, modulus values measured under comparable conditions for pure agarose hydrogels in the 0.3 to 2.0% w/w range are 0.646 to 1.298 kPa [32]. The tensile strength for $Al_{1.5}$–$Ag_{2.3}$, $Al_{1.8}$–$Ag_{2.6}$, and $Al_{2.1}$–$Ag_{2.9}$ were 0.0152 ± 0.0012 MPa, 0.0207 ± 0.0015 MPa, and 0.0328 ± 0.0028 MPa, respectively. The $Al_{2.1}$–$Ag_{2.9}$ ratio was significantly stronger than both other groups proving the reinforcing effect of the agarose-alginate interpenetrating network. This suggests the desired reinforcing behavior of alginate, which makes this hybrid hydrogel more clinically relevant with flexibility and strength. This would probably occur through ionic association of Ca^{2+} to the carboxylate ($-COO^-$) functional groups along the alginate chain, creating greater cross-link density and forces in the polymer network [34]. The agarose network amongst the double network dissipates energy while the soft nature of alginate preserves credibility of the macroscale structure [35-37].

Table 1. Comparison of Young's modulus values of alginate-agarose with related hydrogel systems reported in literature

Hydrogel System	Young's Modulus (kPa)	Reference
Pure Agarose Hydrogel (0.3–2.0% w/w)	0.646–1.298	Jayashankar et al., 2021 [33]
Alginate Hydrogel (Ca^{2+}-crosslinked)	18.5 ± 3.4	Malektaj et al., 2023 [34]
$Al_{1.5}$–$Ag_{2.3}$ (1.5% Alginate / 2.3% Agarose)	15.2	Present study
$Al_{1.8}$–$Ag_{2.6}$ (1.8% Alginate / 2.6% Agarose)	20.7	Present study
$Al_{2.1}$–$Ag_{2.9}$ (2.1% Alginate / 2.9% Agarose)	32.8	Present study
Agarose–Collagen Composite Hydrogel	7.8 ± 1.2	Cambria et al., 2020 [16]
Agarose–Collagen Composite Hydrogel	12.4 ± 2.1	Zigan et al., 2025 [17]

In the present study, the values of the Young's modulus (15.2–32.8 kPa) were significantly higher than those reported for pure agarose hydrogels (0.646–1.298 kPa) [33], confirming the reinforcing effect of alginate incorporation and calcium-mediated crosslinking. The modulus values were also comparable to those reported for other polysaccharide-based hydrogel systems, such as agarose-collagen composite hydrogels and calcium-crosslinked alginate hydrogels [16, 17, 34]. The observed increase in stiffness with increasing polymer concentration is in consistent with previous studies that reported that increased crosslink density and polymer network interconnectivity lead to improved mechanical performance of hydrogels. The results suggest that the developed alginate-agarose hydrogels have mechanical properties suitable for potential wound dressing and tissue engineering applications.

The FT-IR of alginate agarose nanocomposite hydrogel (Figure 2A-C) show broad O-H stretching peaks in the 3000 to 3500 cm^{-1} region and characteristic peaks in the 1500 to 2000 cm^{-1} region and bands below 1000 cm^{-1}, which are typical for polysaccharide backbone vibrations. The broad O-H band suggests significant H-bonding, which is consistent with the alginate–agarose systems reported by Jayashankar et al. (2021) to be due to intermolecular H-bonding and a major factor of miscibility and structural homogeneity in the blended biopolymer [33]. In addition, the peaks observed at 1638-1642 cm^{-1}, is attributed to the asymmetric stretching vibration of carboxylate (COO-) groups. The position and intensity of this band suggest intermolecular interactions within the polymeric network which also show in the observations of Pragya et al. (2021) on the created engineered scaffolds of agarose-based biopolymers [38]. It is also shown that the C-C stretching band of 1200 to 1370 cm^{-1} apparent in the FTIR spectra of individual polymers is absent in the composite and is a clear indication of integrated crosslinked network formation instead of simple physical mixing. In short, the spectrum consolidation indicates chemical compatibility and structural blending or crosslinking leading to uniform material properties in the hydrated state has also been reported in the case of agarose-collagen composites reported by Jayashankar et al. (2021) and Cambria et al. (2020) where FTIR analysis indicated full structural blending with improvement in biofunctionality and applicability of the composites for bone tissue engineering applications [16,33].

The evident reorganization of carboxylate band (1633 to 1642 cm^{-1}) and almost diminished O–H signals in non-citrate paths in silver-incorporated composites approaching silver-carboxylate ($Ag-COO^-$) coordination and stronger metal-polymer interactions. Similar trends were observed in the AgNP-loaded hydrogels by Kumar et al. (2021), in which FTIR analysis indicated the formation of metal-carboxylate coordinated interaction as an essential factor of antimicrobial performance [39]. The developed

molecular features are in a very close association with the mechanical and hydraulic behaviors: the increased values of cross-linking density and detailed coordinated interactions to the high modulus (Figure 2H) and decreased swelling (Figure 2G), which agree with the data manifested by Bardajee et al. (2024), that the enhanced nanocomposite hydrogels were much better mechanical strength and processability over the regular hydrogel material [40]. The swelling capacity of the bionanocomposites was found to be significantly influenced by the Al:Ag ratio. The $Al_{1.8}$-$Ag_{2.6}$ group showed an optimized swelling of 12.8% ± 0.9%, which was statistically higher than the $Al_{1.5}$-$Ag_{2.3}$. The $Al_{2.1}$-$Ag_{2.9}$ showed the lowest degree in swelling compared to other two percentages of composite hydrogel beads. According to the findings, The reduction in the swelling capacity of the $Al_{2.1}$-$Ag_{2.9}$ formulation is related to the increased density of the polymer network. Agarose is a stiff non-swelling double helix which is inherently water-resistant. Meanwhile, the increasing alginate concentration increases the density of carboxylate (-COO−) groups, which results in the stronger ionic coordination and physical cross-linking. The combined effects lead to a tighter more rigid hydrogel matrix that prevents hydraulic expansion. The inclusion of agarose successfully stabilized the alginate network, preventing premature disintegration while maintaining high hydration level. All the data in Figure 2 support the chemical nanoscale regulation of ionic coordination, hydrogen bond interactions, and nanoparticles.

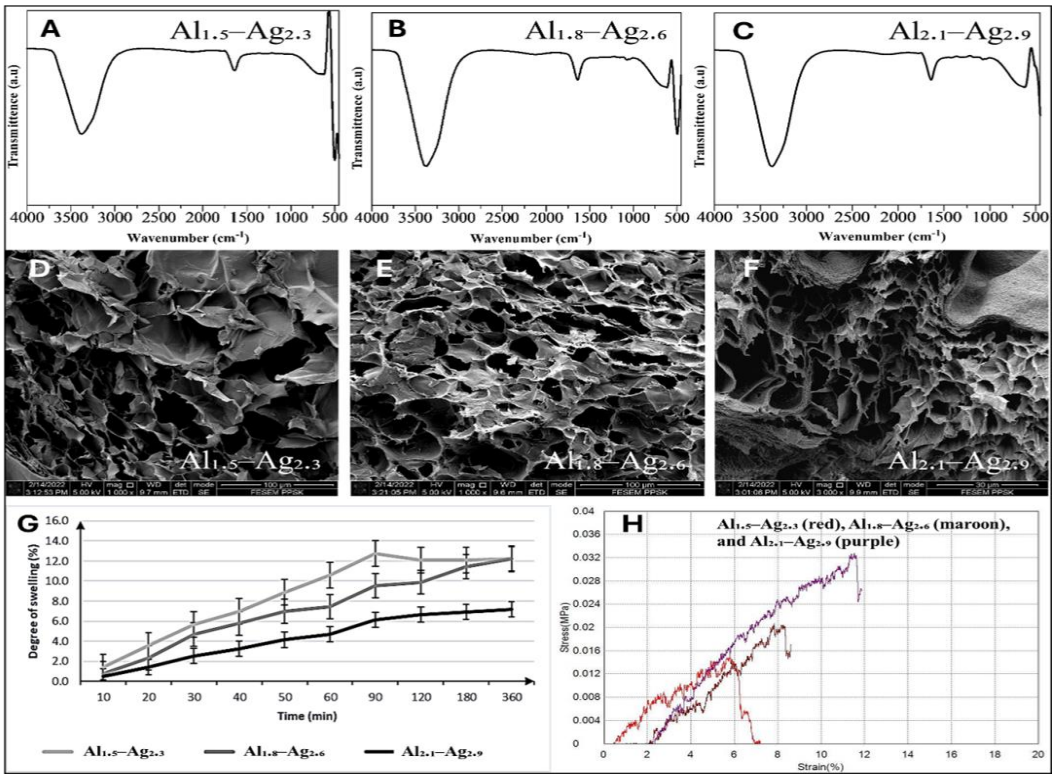

Figure 2. Characterization of alginate–agarose composite hydrogels. (A–C) FT-IR spectra for $Al_{1.5}$–$Ag_{2.3}$, $Al_{1.8}$–$Ag_{2.6}$ and $Al_{2.1}$–$Ag_{2.9}$ showing O–H stretching (3000 to 3500 cm^{-1}) and asymmetric carboxylate (COO^-) stretching vibrations at 1638 to 1642 cm^{-1} bands. (D–F) SEM images reveal porous structures with decreasing porosity as polymer concentration increases. Scale bars: D and E = 100 µm; F = 30 µm. (G) Swelling ratio in 0.3 M phosphate-buffered saline (PBS).

UV-Vis Spectroscopy Analysis of Silver Nitrate Solution

Figure 3 shows the UV–Vis absorption spectra of silver nitrate solutions with and without trisodium citrate (TSC) as a reducing and stabilizing agent. All samples presented a characteristic surface plasmon resonance (SPR) peak between 370 and 410 nm, which confirms AgNP formation. Additional bands between 200 and 350 nm correspond to ligand-centered transitions. Minor peaks around 300 nm are due to nitrate ions. Solving 0.06 M (black), 0.09 M (red) and 0.12 M (blue) silver nitrate are plotted, where solid lines are solutions without trisodium citrate and dashed lines are solutions with trisodium citrate. The broad SPR peak is due to scattering from larger particles. The spectra of no trisodium citrate solutions after the immersion of alginate–agarose beads for 24 hours are similar to the trisodium citrate spectra with the general decrease in the region around 300 nm and an increase in absorbance in the region of 350 and 400 nm, indicating AgNP formation in-situ. It confirms that sodium alginate was able to act as a reducing agent and reduce Ag^+ to AgNPs even in the case of no

trisodium citrate as reducing agent present.

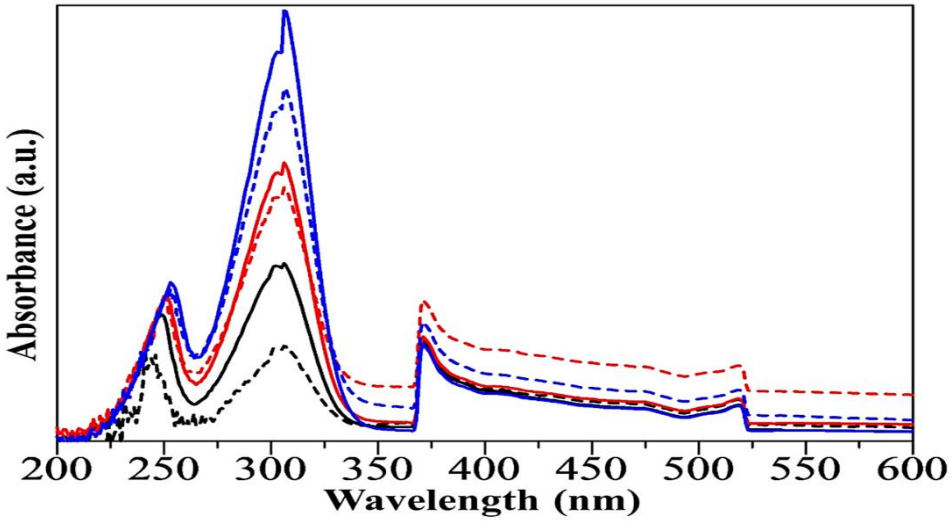

Figure 3.UV–Vis spectra of Ag^+ solutions with and without trisodium citrate. Spectra for 0.06 M (black), 0.09 M (red), and 0.12 M (blue) silver nitrate solutions are shown; solid lines indicate samples without trisodium citrate, dashed lines with TSC. SPR peaks at 370 to 410 nm confirm AgNP formation, while additional peaks near 300 nm correspond to nitrate ions. Similar spectra after hydrogel immersion indicate alginate reduced Ag^+ to AgNPs.

Morphological Features of Alginate–Agarose Beads with and without Silver Nanoparticle Incorporation

Another Colorimetric behavior of alginate–agarose composite hydrogel beads loaded with silver performed differently from the silver-free beads (Figure 4A–C). The transparent beads, after being exposed to the silver nitrate solution, became pale white (Figure 4B) in a very short time, which was common to all formulations. This behavior could be used as an indication of Ag^+ ions reduction into their metal oxides or AgNPs, which are typically known for their characteristic color. Further, while being stored under ambient conditions, the beads turned from white to brownish black to deep black (Figure 4C). This process also indicated the formation of nanoparticles continuously in the hydrogel matrix over time. These observations are evidence of the inclusion of silver in the polymer matrix and the subsequent physicochemical interactions amongst the ionic and polymeric species.

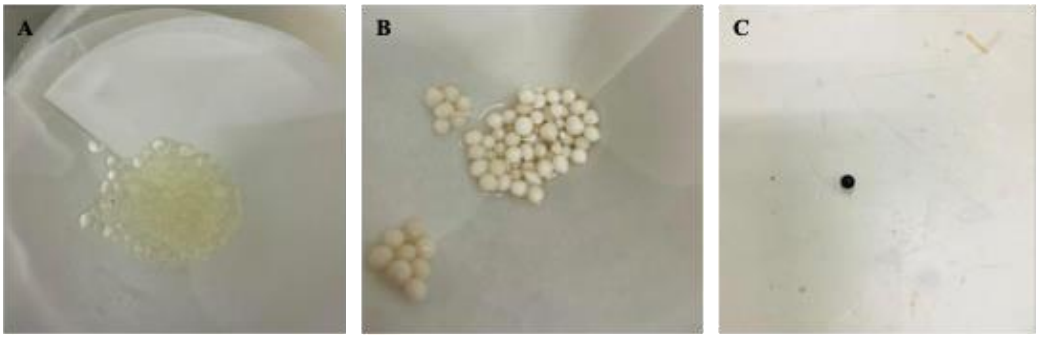

Figure 4. Physical appearance of alginate–agarose composite hydrogel beads before and after silver incorporation. (A) Pure alginate–agarose beads exhibiting a transparent to slightly yellowish hue. (B) Beads after immersion in silver nitrate solution, showing a uniform pale white coloration indicative of initial silver ion interaction. (C) Bead embedded with silver nanoparticles after ambient storage, displaying a deep black colour due to progressive reduction of Ag^+ ions and nanoparticle formation.

Characterisation of Alginate-Agarose embedded with Ag-NPs with/without Trisodium Citrate

Alginate-Agarose embedded with AgNPs prepared without trisodium citrate shown in Figure 5A–C has

FESEM micrographs of alginate–agarose composite hydrogel beads containing silver nanoparticles at the concentrations of $AgNO_3$ at 0.06 M, 0.09 M and 0.12 M. In all samples, well-defined interconnected porous structures were observed, indicating that the presence of silver did not affect the architecture of the hydrogel. The silver nanoparticles were homogenously dispersed in the matrix, and a spherical -like shape was observed at higher magnifications. With increasing $AgNO_3$ concentration from 0.06 M to 0.09 M, particle density and size increased, and 0.12 M gave rise to the highest particle density, and particles could be seen even at lower magnification. Overall, these observations demonstrate that higher Ag^+ concentrations facilitate the formation of larger particles and loss of size control at higher precursor concentrations.

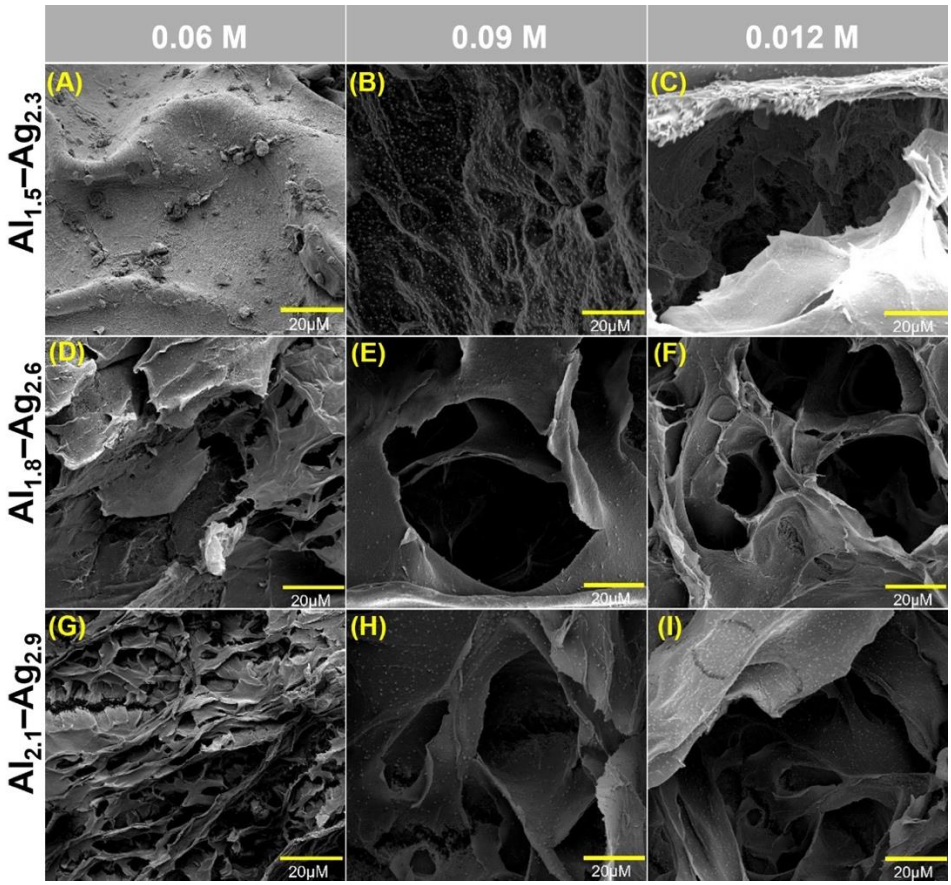

Figure 5.FESEM images at x5,000 magnifications of alginate–agarose composite hydrogel beads embedded with silver nanoparticles synthesized without trisodium citrate. The rows represents the hydrogel formations $Al_{1.5}$–$Ag_{2.3}$ (A-C) , $Al_{1.8}$–$Ag_{2.6}$ (D-F), and $Al_{2.1}$–$Ag_{2.9}$ (G-I), while the columns corresponds to the $AgNO_3$ concentrations used during silver nanoparticle synthesis (0.06, 0.09 and 0.12 M). Scale bars = 20μm.

Meanwhile, FESEM images shown in Figure 6 of alginate–agarose composite hydrogel beads, prepared with trisodium citrate, show that all formulations $Al_{1.5}$–$Ag_{2.3}$ (6A-6C); $Al_{1.8}$–$Ag_{2.6}$ (6D-6F); $Al_{2.1}$–$Ag_{2.9}$ (6G-6I) maintained highly interconnected porous structures. This indicates that immersion in silver nitrate culture and subsequent incorporation of silver nanoparticles did not disturb the hydrogel architecture. Silver particles assumed a spherical morphology and were homogeneously distributed throughout the hydrogel matrix without agglomeration. At 0.06 (Figure 6A), these spherical were smaller than the non-citrate samples, while increasing concentrations, 0.09 M and 0.12 M (Figures 6B–C), were progressively larger in size with increasing Ag^+ concentration. Thus, trisodium citrate appears to be a stabilizing agent that did not disturb the hydrogel architecture, while the effect on the resulting particle size, that is, spherical, was small and perhaps masked by the reducing capacity of the alginate. Thus, increasing Ag^+ concentrations dictate the size of the resulting AgNPs in both citrate and non-citrate series, but overall did not affect the apparent regular distribution of AgNPs and robust hypothesized pore architecture.

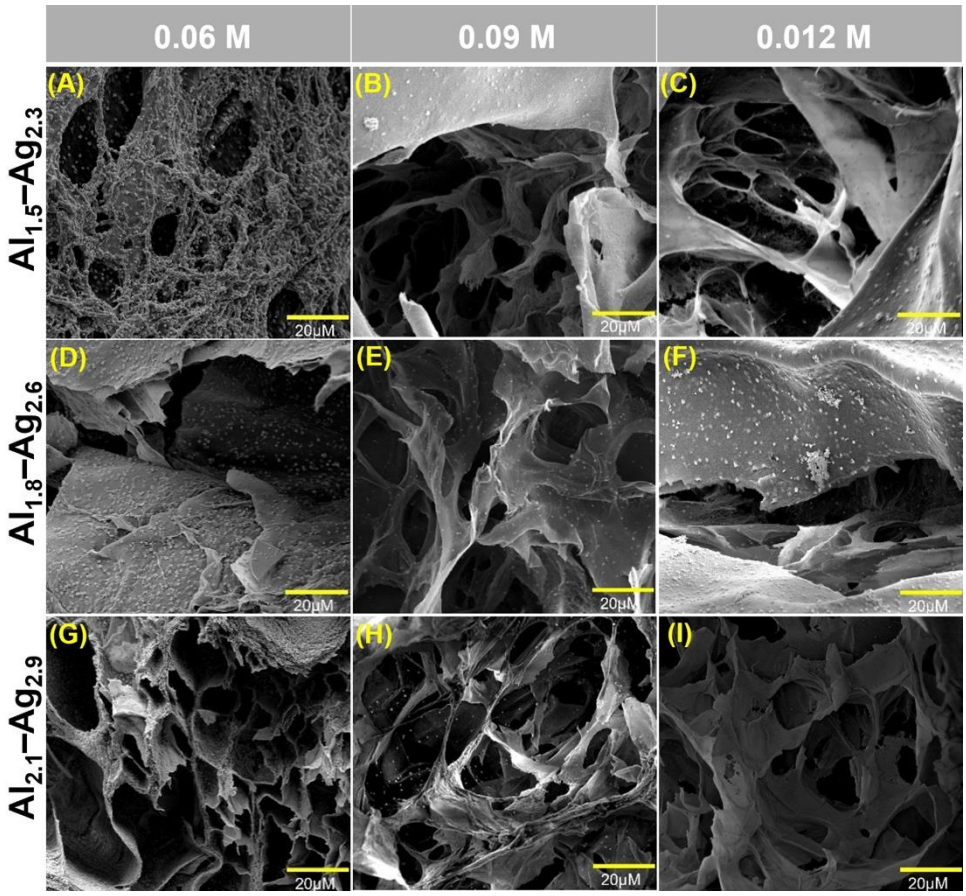

Figure 6. FESEM images at x5,000 magnifications of alginate–agarose composite hydrogel beads embedded with silver nanoparticles synthesized with trisodium citrate. The rows represents the hydrogel formations $Al_{1.5}$–$Ag_{2.3}$ (A-C), $Al_{1.8}$–$Ag_{2.6}$ (D-F), and $Al_{2.1}$–$Ag_{2.9}$ (G-I), while the columns corresponds to the $AgNO_3$ concentrations used during silver nanoparticle synthesis (0.06, 0.09 and 0.12 M). Scale bars = 20µm.

FTIR Spectroscopy Analysis with/without Trisodium Citrate

Figure 7A–F shows the FTIR spectra of the Al-Ag composite hydrogel beads synthesized by two different methods (citrate-assisted and non-citrate). Three formulations ($Al_{1.5}$–$Ag_{2.3}$, $Al_{1.8}$–$Ag_{2.6}$, $Al_{2.1}$–$Ag_{2.9}$) were studied at three different concentrations (0.06, 0.09 and 0.12 M) of silver. Hydrogen bonding is evident from the O-H stretching band on the high wavenumber side of 3000-3500 cm^{-1}, Ag-carboxylate coordination from the carboxylate/carbonyl region at 1633-1642 cm^{-1} and integrity of the polysaccharide backbone from the backbone features at 1327 and 1077 cm^{-1}. In the citrate-assisted samples (Figure 7A–C), an O-H band at approximately 3300 cm^{-1} indicates the stabilization of the hydrated network by citrate ions. Notably, the peak of 0.06 M is sharper compared to the 0.09 M and 0.12 M concentrations for all the nanocomposite hydrogels for these citrate-assisted samples, suggesting specific coordination dynamics of Ag-COO^- species at this concentration.

The backbone bands remain visible, indicating that the polysaccharide network is still intact. The glycosidic vibration at 1077 cm^{-1} is characteristic of the high agarose containing samples. In the non-citrate group (Figure 7D–F) there is a more direct interaction between the silver ions and the polymeric chains. The intensity of the O-H band is reduced at 0.06 M indicating a stronger ion binding of the Ag^+ cations to the hydroxyl and carboxylate groups. Furthermore, the band at 1633 cm^{-1} is indicative of the presence of the coordinated Ag-COO^- complexes.

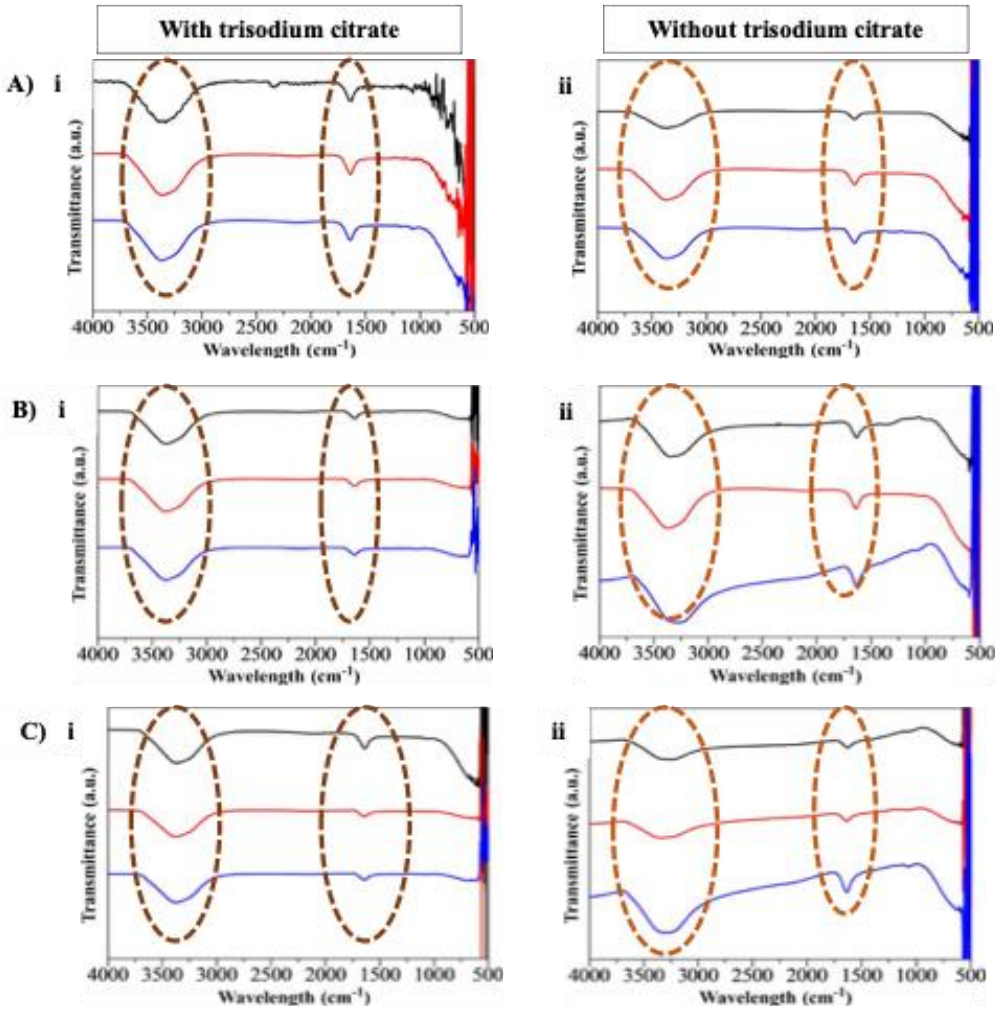

Figure 7.FTIR spectra of alginate–agarose composite hydrogel beads embedded with silver nanoparticles synthesised A-C (i) with the reducing agent, trisodium citrate and A-C (ii) without a reducing agent. Panels A-C corresponds to $AgNO_3$ concentrations of 0.06M (A), 0.09M (B), and 0.12M (C).

Selection of Optimal Formulation

The elemental composition of the biosynthesized composite hydrogel beads was analyzed using Energy-Dispersive X-ray (EDX), where Figure 8A–C represent samples prepared with 0.06 M, 0.09 M, and 0.12 M $AgNO_3$, respectively.

All spectra exhibited a characteristic silver peak at 3 keV, confirming the formation of silver nanoparticles within the hydrogel matrix. Moreover, quantitative analysis revealed concentration-dependent variations, with silver contents of 15.17 wt%, 7.11 wt%, and 11.45 wt%, while corresponding changes in carbon and oxygen indicated progressive nanoparticle loading and dispersion. Overall, these results confirm the successful incorporation and uniform distribution of silver nanoparticles, with higher precursor concentrations producing greater nanoparticle content. Subsequently, Transmission Electron Microscopy (TEM) analysis (Figure 9A–H) showed that nanoparticles ranged from 6.6 to 22.9 nm (average 14.1 nm) and were predominantly spherical or ellipsoidal, with most particles below 50 nm, indicating uniform dispersion and structural stability.

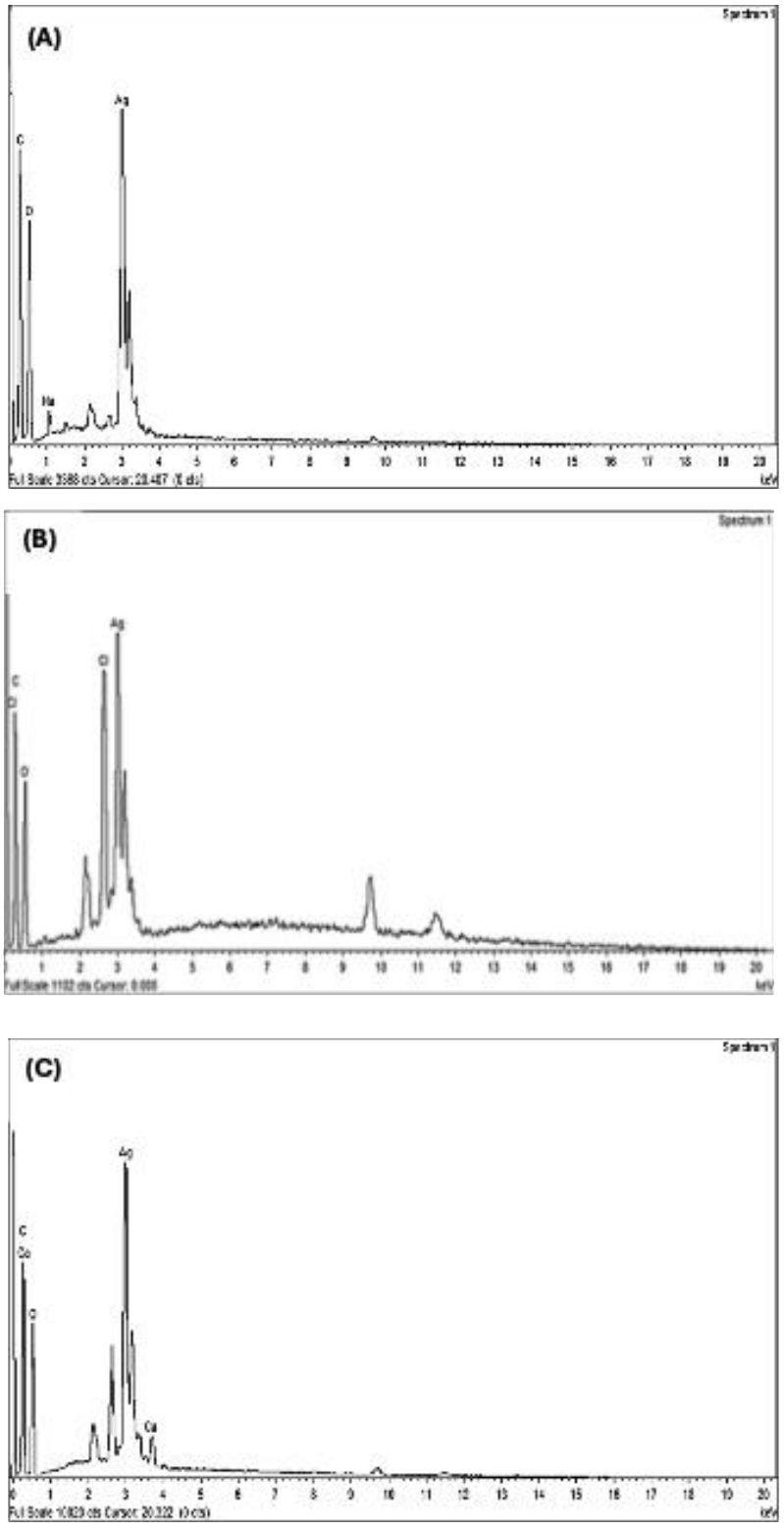

Figure 8. Energy Dispersive X-ray (EDX) spectra of optimized alginate–agarose composite hydrogel beads ($Al_{1.8}$–$Ag_{2.6}$) embedded with silver nanoparticles at varying silver nitrate concentrations (A) 0.06M, (B) 0.09M and (C) 0.12M.

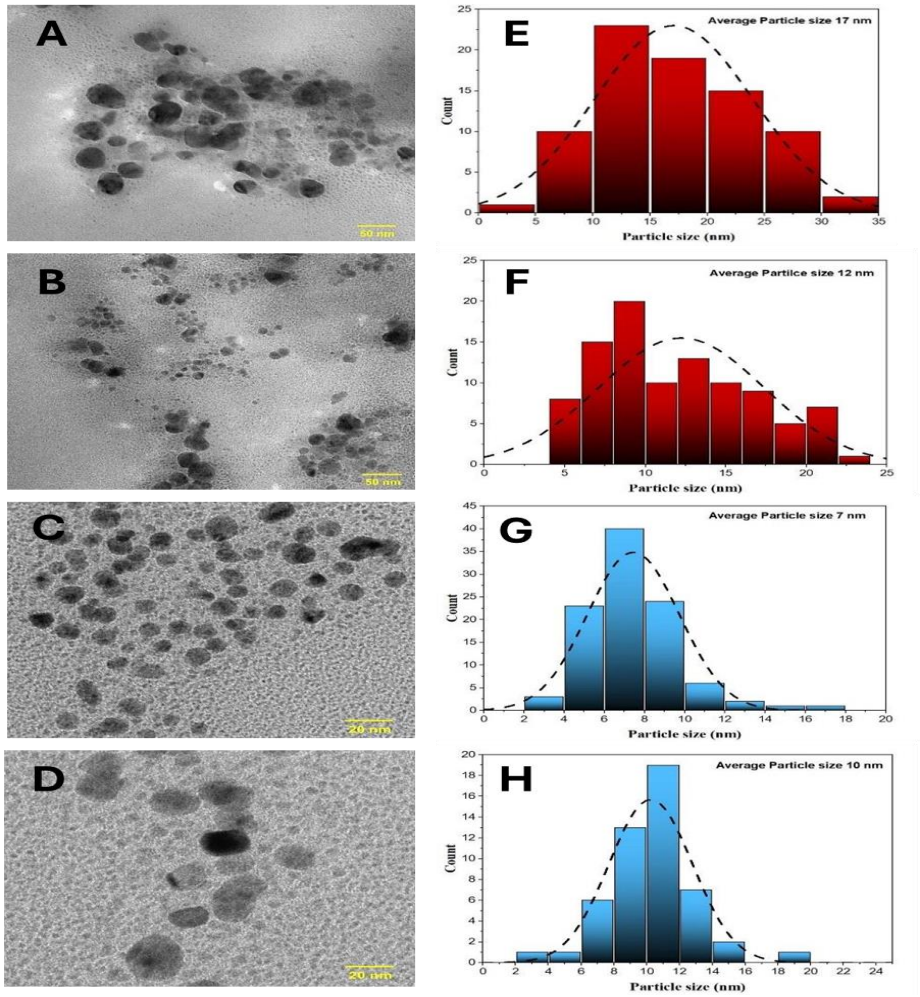

Figure 9.TEM micrographs and particle size distribution of silver nanoparticles embedded in alginate–agarose composite hydrogels. Panels A–D show TEM images of silver nanoparticles incorporated into hydrogel matrices under different conditions, revealing predominantly spherical morphology with uniform dispersion. Panels E–H present corresponding particle size distribution histograms, indicating average particle sizes of 17 nm (E), 12 nm (F), 7 nm (G), and 10 nm (H). Scale bars = 20 nm.

Antibacterial Activity

The antibacterial activity of silver nanoparticle (AgNP) loaded alginate–agarose composite hydrogel beads was assessed against Gram-positive bacterium *Staphylococcus aureus* (S. aureus) and Gram-negative bacteria *Escherichia coli* (E. coli) and *Pseudomonas aeruginosa* (P. aeruginosa). The antibacterial performance was first studied by the Kirby–Bauer disc diffusion assay at three different silver concentrations (0.06, 0.09 and 0.12 M) (Figure 10A–C).

The pure alginate–agarose hydrogel beads ($Al_{1.8}$–$Ag_{2.6}$) did not exhibit inhibition zones against any of the tested bacterial strains, indicating that the hydrogel matrix has no antibacterial activity. In contrast, AgNP-loaded hydrogels showed measurable antibacterial activity against all the tested bacterial strains. The inhibition zones for S. aureus were 4.1 mm (Al–Ag–1), 4.8 mm (Al–Ag–2) and 4.1 mm (Al–Ag–3) in comparison to 18.7 mm for the positive control. For E. coli the same trend was observed with inhibition zones of 4.4, 4.8, and 5.1 mm for Al–Ag–1, Al–Ag–2, and Al-Ag-3, respectively, while the positive control gave a zone of 19.2 mm. The largest inhibition zones were observed for P. aeruginosa with values of 7.0 mm for Al–Ag–1 and Al–Ag–3 and 8.3 mm for Al–Ag–2, while the positive control showed 14.3 mm. Increasing the silver concentration beyond 0.09 M did not lead to a significant increase in the inhibition zone diameter indicating that the antibacterial performance reached a plateau under the tested conditions. Generally, the addition of AgNPs increased the antibacterial activity of the alginate–agarose hydrogel and P. aeruginosa was the most sensitive bacterial strain among the tested ones.

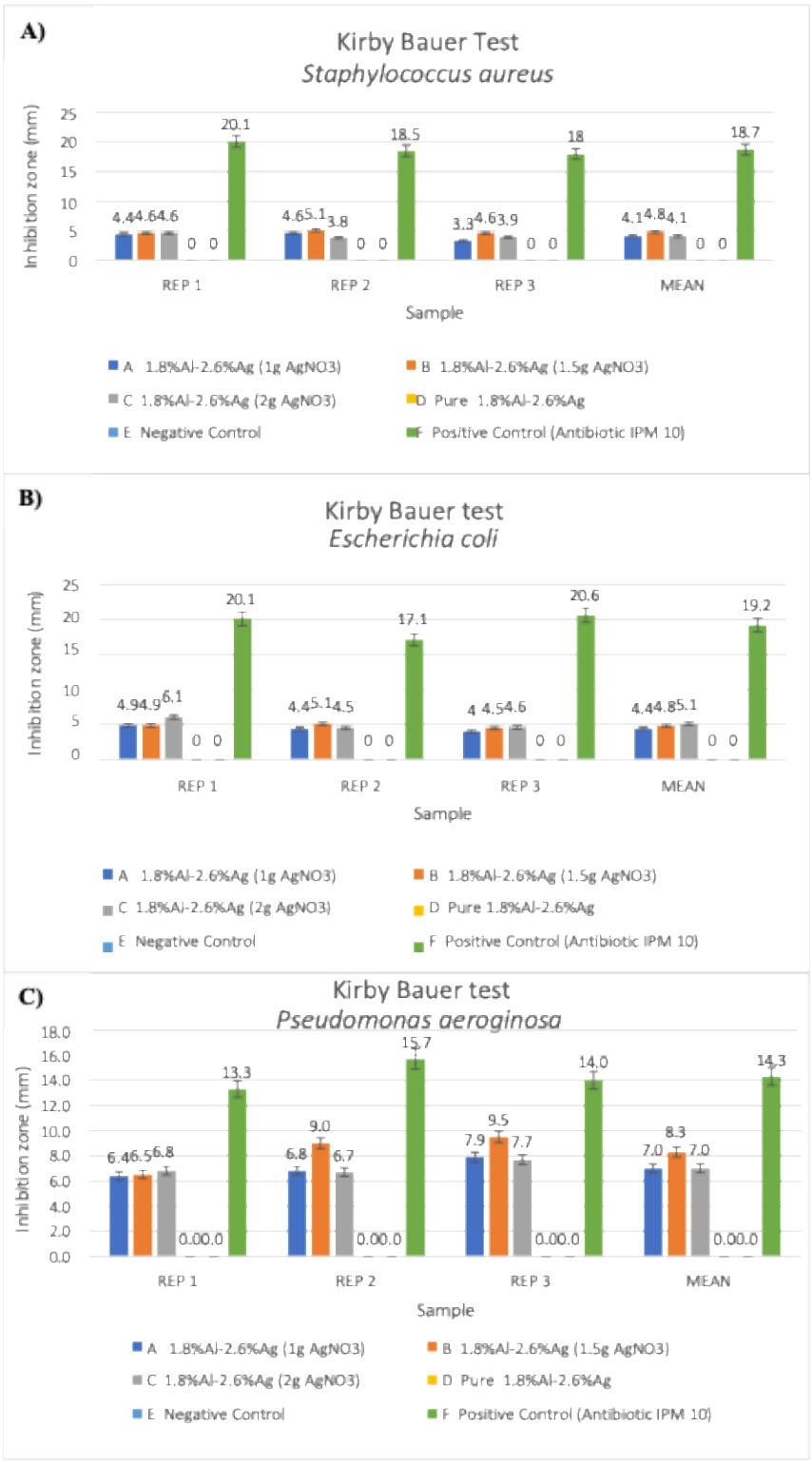

Figure 10. Antibacterial activity of alginate–agarose composite hydrogels with and without silver nanoparticles against Gram-positive and Gram-negative bacteria. Kirby–Bauer disc diffusion assay showing zones of inhibition (ZOI) for pure composite hydrogel ($Al_{1.8}$–$Ag_{2.6}$) and silver-loaded variants containing 1.0 g (A), 1.5 g (B), and 2.0 g (C) $AgNO_3$. Negative control (E) exhibited no inhibition, while positive control (F) produced the largest ZOI.

To further evaluate the antibacterial activity, Total Plate Count (TPC) analysis was carried out after 24 h of exposure to the hydrogel formulations (Table 2). All the AgNP-loaded formulations (Al–Ag–1 (0.06 M), Al–Ag–2 (0.09 M) and Al–Ag–3 (0.12 M)) showed total inhibition of bacterial growth and no colonies were found (0 CFU mL-1) for all the microorganisms tested. In contrast, the pure alginate-agarose beads (Sample D), the negative control (Sample F), and the sterilised beads (Sample G) showed a significant growth of bacteria, supporting the absence of antibacterial activity in the hydrogel matrix itself. These results suggest that the antibacterial effect observed was due to the incorporation of silver nanoparticles.

The antibacterial activity of the nanocomposite hydrogels was further studied using Kirby–Bauer disc diffusion and total plate count (TPC) tests. The antibacterial activity of the AgNP-loaded hydrogels was verified by the Kirby–Bauer assay, where inhibition zones of 4.1–8.3 mm were observed. However, the inhibition zones were much smaller than those observed for the positive control, suggesting moderate diffusion-mediated antibacterial effects. This observation can be related to the poor diffusion of silver species from the highly crosslinked hydrogel network into the surrounding agar medium. Similar results have been reported for AgNP-incorporated hydrogel systems where the polymeric matrix limits the mobility of the nanoparticles and slows the release of bioactive silver ions compared to traditional antibiotic agents.

In contrast, the TPC assay showed complete bacterial inhibition with no viable colonies detected (0 CFU mL^{-1}) after direct exposure of the AgNP-containing hydrogels. The difference between the results of the Kirby-Bauer and TPC suggests that the antibacterial efficacy is not only dependent on the diffusion of the antimicrobial agents in the surrounding environment. Instead, the results show that the bacterial inactivation is mainly due to the direct interaction between bacterial cells and the surface of the AgNP-loaded hydrogel and the localised interactions play an important role in the antimicrobial activity. However, the contribution of prolonged silver ion release cannot be excluded. Collectively, these results indicate that the antibacterial mechanism of the developed nanocomposite hydrogels is governed by a synergistic combination of contact-mediated bactericidal effects.

Table 2. Summary of Total Plate Count (TPC) Analysis

Sample Identification	S. aureus (CFU/ml)	E. coli (CFU/ml)	P. aeruginosa (CFU/ml)
(A) Al-Ag-1 (0.06M AgNPs)	0	0	0
(B) Al-Ag-2 (0.09M AgNPs)	0	0	0
(C) Al-Ag-3 (0.12M AgNPs)	0	0	0
(D) Pure Al-Ag Beads	6.4×10^8	2.4×10^8	2.3×10^8
(F) Negative Control	8.9×10^8	2.9×10^8	5.5×10^8
(G) Sterilized Pure Beads + Bacteria	4.0×10^8	2.9×10^8	1.5×10^8
(H) Positive Control (IPM 10)	0	0	0

Cell Attachment Assay and Morphological Evaluation of DPSCs on Silver-Loaded Hydrogel

To evaluate the cytocompatibility of the optimized $Al_{1.8}$–$Ag_{2.6}$ hydrogel formulations, dental pulp stem cell (DPSC) attachment and morphological evaluation were conducted using FESEM, shown in Figure 11. The pure alginate–agarose hydrogel (Figure 11A) showed poor cell attachment, with cells clustered in localized areas and unevenly distributed on the surface of the hydrogel. A higher magnification image (Figure 11E) also showed the presence of rounded and contracted cellular morphologies, which are often related to poor cell attachment and reduced cellular viability.

By contrast, the AgNPs-loaded hydrogels with 0.06 M, 0.09 M and 0.12 M of silver nanoparticles (Figure 11B–D) supported the attachment and spreading of DPSCs. Cells had a flat morphology with long cell extensions and were more homogeneously distributed over the surface of the hydrogel than on pure hydrogel. No distinct morphological abnormalities such as membrane blebbing, severe cell shrinkage or extensive cellular fragmentation were observed in the AgNP containing formulations. In general, the presence of flattened and well-spread cells is taken as sign of good cell-material interactions, active cell adhesion and cytocompatibility, whereas rounded and contracted morphologies are often associated with decreased attachment and reduced cell viability [41].

The improved cellular attachment on the AgNPs-loaded hydrogels could be due to the homogeneous and interconnected structure of the alginate-agarose network, providing a good microenvironment for cell-material interactions. Such observations indicate that the presence of silver nanoparticles in the concentration levels used in this study did not have a negative effect on the morphology of DPSCs and promoted the attachment of cells to the surface of the hydrogel. Moreover, the FESEM results revealed that the synthesised nanocomposite hydrogels maintained cytocompatibility and antibacterial functionality, making them potentially suitable for biomedical and wound healing applications.

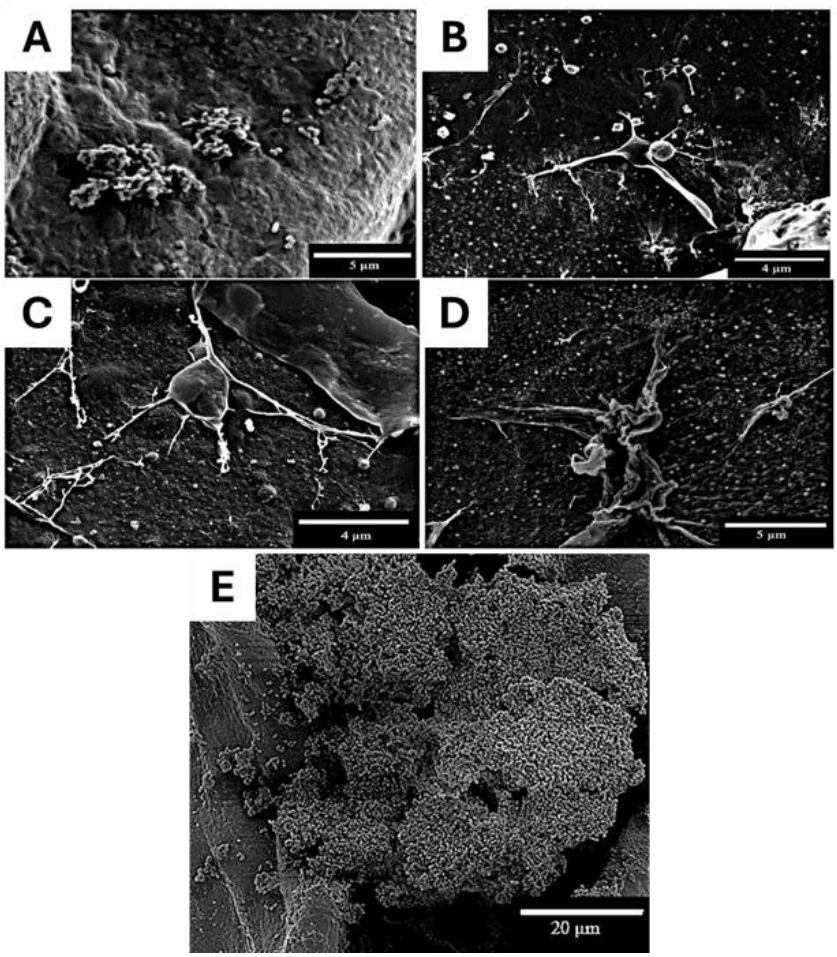

Figure 11. FESEM images showing dental pulp stem cell (DPSC) attachment on composite hydrogels with and without silver nanoparticles. (A) Pure composite hydrogel (1.8% alginate–2.6% agarose) showing poor cell adhesion and early apoptotic morphology. (B–D) Composite hydrogels embedded with silver nanoparticles at concentrations of 0.06 M (B), 0.09 M (C), and 0.12 M (D), exhibiting improved cell spreading and flattened morphology without microvilli or blebs. (E) High-magnification view of cell aggregation on pure hydrogel surface, indicating non-uniform distribution and compromised viability. Scale bars: A and D = 5 µm; B and C = 4 µm; E = 20 µm.

In Vitro Cytotoxicity Assay

The cytocompatibility of the $Al_{1.8}$-$Ag_{2.6}$ nanocomposite was evaluated using HDF cells after 24 hours of exposure to serially diluted nanocomposite extracts. In this study, the treatment range was expressed as nanocomposite extract concentration, namely 100%, 50%, 25%, 10%, and 0%, instead of exact silver concentration because the amount of silver released into the culture medium was not quantified. The preliminary Alamar Blue screening showed that the lowest 0.06 M of silver formulation reduced HDF viability. Therefore, the silver loading was decreased to 0.015 M to improve cellular compatibility [42].

As shown in Figure 12, A repeated-measures one-way ANOVA showed a significant effect of extract concentration on HDF viability with $p = 0.013$. Tukey's test confirmed a clear threshold effect where viability at 50% and 100% was significantly lower than at 5%, 10%, and 25% ($p < 0.0001$), this result statistically confirmed the concentration-dependent cytotoxic trend observed. Higher extract

concentrations produced lower cell viability compared with diluted extracts, indicating a concentration-dependent cellular response. This may be due to greater exposure of cells to soluble components released from the hydrogel matrix during the 24 hours extraction period.

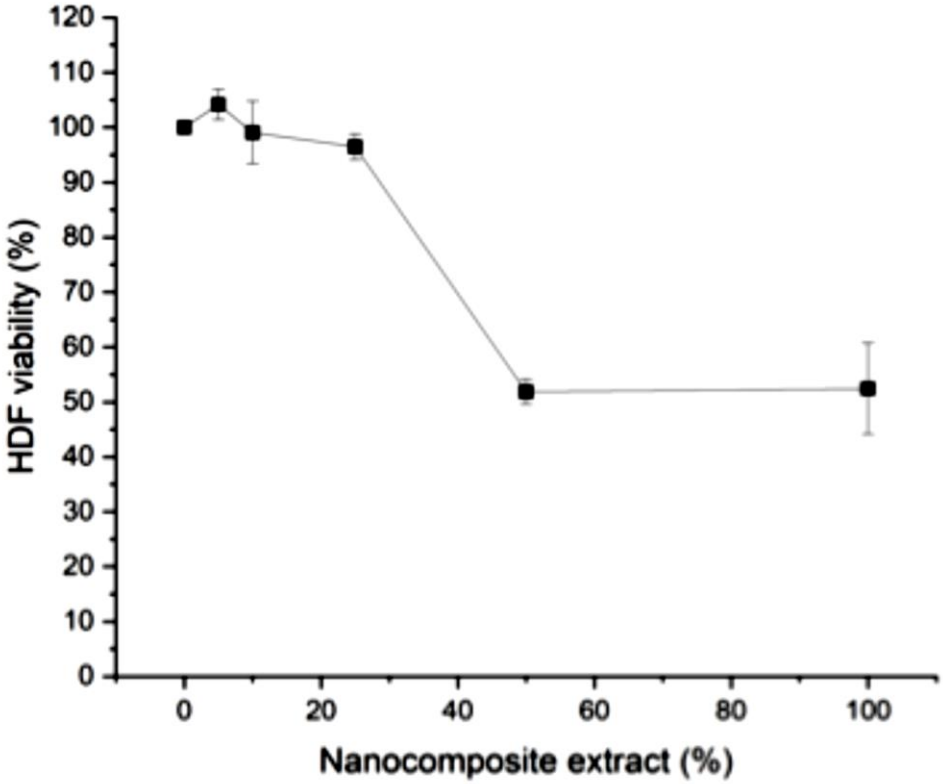

Figure 12. HDF cell viability after 24 hours exposure to nanocomposite extracts at different concentrations. Data are expressed as mean ± SD from three biological replicates. Statistical analysis was performed using one-way ANOVA. A value of $p<0.05$ was considered statistically significant.

This finding agrees with previous studies reporting that silver-based nanomaterials may show concentration-dependent effects on fibroblast viability, depending on the silver dose, exposure time, particle stabilisation, and interaction with the surrounding matrix [43,44]. Similarly, previous studies have demonstrated that polysaccharide-based matrices can effectively support the incorporation of silver nanoparticles for wound dressing applications while maintaining acceptable biological performance [45]. In the present study, the alginate/agarose matrix may have reduced direct interaction between silver nanoparticles and HDF cells, although this should be confirmed by future silver release analysis. Overall, reducing the silver loading from 0.06 M to 0.015 M improved the cytocompatibility profile of the nanocomposite. The diluted extracts showed better compatibility with HDF cells, supporting the suitability of the optimised formulation for further wound dressing evaluation.

While these finding demonstrates promising cytocompatibility, it is important to consider certain limitation to the present study. We acknowledge that our present study lacks Ag^{+} release kinetics, degradation behaviour and long-term stability of the developed hydrogel system which are crucial parameters to evaluate the silver containing biomaterials as ion release and stability can affect their antibacterial performance as well as the biological responses. Since it is an initial study focussing on the development and primary functionality of Alginate–Agarose silver Nanocomposites Hydrogels these aspects were not considered in detail and we understand that but will be taken up in our future works by investigating silver ions release profiles, degradation behaviour and long term stabilities to reinforce and expand our present findings and facilitate the optimisation studies.

Conclusion

The present study reports the successful fabrication and optimization of alginate–agarose silver nanocomposite hydrogels for possible wound dressing applications. The embedding of agarose within the alginate matrix enhanced the structural stability and mechanical performance of the hydrogel whereas the in-situ generation of silver nanoparticles imparted potent antibacterial functionality. Physicochemical characterization confirmed the successful formation of a porous and interconnected hydrogel network with silver nanoparticles uniformly distributed in the polymer matrix. Statistical analysis showed that the swelling behavior, mechanical properties, and overall performance of the hydrogels were significantly affected by the differences in polymer composition.

Among all the formulations tested, $Al_{1.8}$–$Ag_{2.6}$ showed the most promising results in terms of optimum swelling capacity, adequate mechanical strength and biological response. The $Al_{2.1}$-$Ag_{2.9}$ formulation was significantly more tensile strength but without a corresponding improvement in swelling performance or cellular response indicating that increasing the polymer concentration beyond the optimised level did not necessarily improve the overall functionality.

The incorporation of silver nanoparticles imparted remarkable antibacterial activity against Gram-positive as well as Gram-negative bacterial strains. The Kirby-Bauer analysis showed that the nanocomposite hydrogels have moderate antibacterial effects by diffusion, while the total plate count analysis revealed that they completely inhibited bacterial growth after direct contact, demonstrating their strong antimicrobial potential. Further cytocompatibility evaluation demonstrated a concentration-dependent cellular response. The viability of HDFs significantly decreased at higher extract concentrations, while diluted extracts showed more suitable compatibility with cells. Interestingly, the cytocompatibility profile of the optimised formulation was enhanced with a reduction in silver loading from 0.06 M to 0.015 M, while keeping its antibacterial efficacy.

In summary, the optimised $Al_{1.8}$–$Ag_{2.6}$ nanocomposite hydrogel has favourable swelling properties, mechanical strength, antibacterial activity and enhanced cytocompatibility, suggesting its potential use for advanced wound dressing applications. The results of this study provide useful information on the design and optimisation of multifunctional biopolymer-based nanocomposite hydrogels for biomedical application. Further studies will be carried out on the Ag^+ release kinetics, degradation behaviour and long-term stability to confirm the long-term performance, safety and clinical potential of the developed alginate–agarose silver nanocomposite hydrogels for wound dressing applications.

Conflicts of Interest

The author(s) declare(s) that there is no conflict of interest regarding the publication of this paper.

Acknowledgment

This work is part of a research Universiti Sains Malaysia (USM), through short term research grant (304/PPSG/6315509) and the authors thanked the School of Dental Sciences, Universiti Sains Malaysia for providing the facility to conduct this study.

References

[1] Zhang YS, Khademhosseini A. Advances in engineering hydrogels. Science. 2017 May 5;356(6337).
[2] Correa S, Grosskopf AK, Lopez Hernandez H, Chan D, Yu AC, Stapleton LM, et al. Translational Applications of Hydrogels. Chemical Reviews. 2021 May 3;121(18):11385–457.
[3] Yang J, Yu H, Wang L, Liu J, Liu X, Hong Y, et al. Advances in adhesive hydrogels for tissue engineering. European Polymer Journal. 2022 Jun;172:111241.
[4] Catoira MC, Fusaro L, Di Francesco D, Ramella M, Boccafoschi F. Overview of natural hydrogels for regenerative medicine applications. Journal of Materials Science: Materials in Medicine. 2019 Oct;30(10).
[5] Ahmed EM. Hydrogel: Preparation, characterization, and applications: A review. Journal of Advanced Research. 2015 Mar;6(2):105–21.
[6] He J, Sun Y, Gao Q, He C, Yao K, Wang T, et al. Gelatin Methacryloyl Hydrogel, from Standardization, Performance, to Biomedical Application. Advanced Healthcare Materials. 2023 May 15;12(23).
[7] Chaudhuri O, Cooper-White J, Janmey PA, Mooney DJ, Shenoy VB. Effects of extracellular matrix viscoelasticity on cellular behaviour. Nature. 2020 Aug 26;584(7822):535–46.
[8] Shang S, Zhuang K, Chen J, Zhang M, Jiang S, Li W. A bioactive composite hydrogel dressing that promotes healing of both acute and chronic diabetic skin wounds. Bioactive Materials. 2024 Apr;34:298–310.
[9] GhavamiNejad A, Park CH, Kim CS. In Situ Synthesis of Antimicrobial Silver Nanoparticles within Antifouling

Zwitterionic Hydrogels by Catecholic Redox Chemistry for Wound Healing Application. Biomacromolecules. 2016 Mar 1;17(3):1213–23.
[10] Begum F, Mahto AK, Kumari S, Dewangan RP. In-Situ Synthesis of Silver Nanoparticle within Self-Assembling Ultrashort Peptide Hydrogel as Antibacterial with Wound Healing Properties. Current Protein & Peptide Science. 2025 Oct;26(8):667–81.
[11] Joly JP, Aricov L, Balan GA, Popescu EI, Mocanu S, Leonties AR, et al. Formation of Alginate/Chitosan Interpenetrated Networks Revealed by EPR Spectroscopy. Gels. 2023 Mar 16;9(3):231.
[12] Shukla A, Syaifie PH, Rochman NT, Jaya Syaifullah S, Jauhar MM, Mardliyati E. A recent study of natural hydrogels: improving mechanical properties for biomedical applications. Biomedical Materials. 2025 Mar 1;20(2):022010.
[13] Yan X, Huang H, Bakry AM, Wu W, Liu X, Liu F. Advances in enhancing the mechanical properties of biopolymer hydrogels via multi-strategic approaches. International Journal of Biological Macromolecules. 2024 Jun;272:132583.
[14] Liu L, Wang Y, Li X, Li P, Jin Y, Yu H, et al. Recent developments in polysaccharide-based conductive hydrogels: A review and perspective. Carbohydrate Polymers. 2025 Dec;370:124453.
[15] Li Z, Lin Z. Recent advances in polysaccharide-based hydrogels for synthesis and applications. Aggregate. 2021 Jan 19;2(2).
[16] Cambria E, Brunner S, Heusser S, Fisch P, Hitzl W, Ferguson SJ, et al. Cell-Laden Agarose-Collagen Composite Hydrogels for Mechanotransduction Studies. Frontiers in Bioengineering and Biotechnology. 2020 Apr 21;8.
[17] Zigan C, Benito Alston C, Chatterjee A, Solorio L, Chan DD. Characterization of Composite Agarose–Collagen Hydrogels for Chondrocyte Culture. Annals of Biomedical Engineering. 2024 Sep 14;53(1):120–32.
[18] Rana MM, De la Hoz Siegler H. Biocompatibility. Nature-Inspired Sensors. 2025;111–26.
[19] Rahman MdM, Shahid MdA, Hossain MdT, Sheikh MdS, Rahman MdS, Uddin N, et al. Sources, extractions, and applications of alginate: a review. Discover Applied Sciences. 2024 Aug 15;6(8).
[20] Huang Y, Peng S, Chen Y, Chu B. Agarose Hydrogels for Bone Tissue Engineering, from Injectables to Bioprinting. Gels. 2025 Mar 28;11(4):255.
[21] Baishya G, Parasar B, Limboo M, Kumar R, Dutta A, Hussain A, et al. Advancements in nanocomposite hydrogels: a comprehensive review of biomedical applications. Discover Materials. 2024 Aug 28;4(1).
[22] Barrett-Catton E, Ross ML, Asuri P. Multifunctional Hydrogel Nanocomposites for Biomedical Applications. Polymers. 2021 Mar 11;13(6):856.
[23] Pangli H, Vatanpour S, Hortamani S, Jalili R, Ghahary A. Incorporation of Silver Nanoparticles in Hydrogel Matrices for Controlling Wound Infection. Journal of Burn Care & Research. 2020 Dec 12;42(4):785–93.
[24] Nicolae-Maranciuc A, Chicea D. Polymeric Systems as Hydrogels and Membranes Containing Silver Nanoparticles for Biomedical and Food Applications: Recent Approaches and Perspectives. Gels. 2025 Sep 2;11(9):699.
[25] Pranantyo D, Yeo CK, Wu Y, Fan C, Xu X, Yip YS, et al. Hydrogel dressings with intrinsic antibiofilm and antioxidative dual functionalities accelerate infected diabetic wound healing. Nature Communications. 2024 Feb 1;15(1).
[26] Stuermer EK. Wound biofilm: a bacterial success story. Journal of Wound Management Official journal of the European Wound Management Association. 2023 Jul 1;(July 2023).
[27] Shen AZ, Taha M, Ghannoum M, Tyring SK. Biofilms and Chronic Wounds: Pathogenesis and Treatment Options. Journal of Clinical Medicine. 2025 Nov 2;14(21):7784.
[28] Nishiguchi A. Advances in injectable hydrogels with biological and physicochemical functions for cell delivery. Polymer Journal. 2024 Jul 9;56(10):895–903.
[29] Baishya G, Parasar B, Limboo M, Kumar R, Dutta A, Hussain A, et al. Advancements in nanocomposite hydrogels: a comprehensive review of biomedical applications. Discover Materials. 2024 Aug 28;4(1).
[30] Liu Y, Jiang L, Jiang R, Liu H. Versatile nanocomposite hydrogel induced by Au-Se interaction showing mechanically tough and multi-responsive self-healing properties. Journal of Materials Science. 2024 May;59(19):8287–97.
[31] Pangli H, Vatanpour S, Hortamani S, Jalili R, Ghahary A. Incorporation of Silver Nanoparticles in Hydrogel Matrices for Controlling Wound Infection. Journal of Burn Care & Research. 2020 Dec 12;42(4):785–93.
[32] Liu Y, Yu D, Han H, Jia H. NIR-responsive nano-photothermal and antioxidant platforms to combat bacteria. Science China Materials. 2025 May 12;68(6):2111–21.
[33] Xiang Ping MK, Zhi HW, Aziz NS, Hadri NA, Ghazalli NF, Yusop N. Optimization of agarose–alginate hydrogel bead components for encapsulation and transportation of stem cells. Journal of Taibah University Medical Sciences. 2023 Feb;18(1):104–16.
[34] Malektaj H, Drozdov AD, deClaville Christiansen J. Mechanical Properties of Alginate Hydrogels Cross-Linked with Multivalent Cations. Polymers. 2023 Jul 12;15(14):3012.
[35] Liang Z, Liu C, Li L, Xu P, Luo G, Ding M, et al. Double-Network Hydrogel with Tunable Mechanical Performance and Biocompatibility for the Fabrication of Stem Cells-Encapsulated Fibers and 3D Assemble. Scientific Reports. 2016 Sep 15;6(1).
[36] Narayana S, Gowda BHJ, Hani U, Ahmed MG, Asiri ZA, Paul K. Smart Poly(N-isopropylacrylamide)-Based Hydrogels: A Tour D'horizon of Biomedical Applications. Gels. 2025 Mar 15;11(3):207.
[37] Miskovic V, Malafronte E, Minetti C, Machrafi H, Varon C, Iorio CS. Thermotropic Liquid Crystals for Temperature Mapping. Frontiers in Bioengineering and Biotechnology. 2022 May 12;10.
[38] Pragya A, Mutalik S, Younas MW, Pang SK, So PK, Wang F, et al. Dynamic cross-linking of an alginate–acrylamide tough hydrogel system: time-resolved in situ mapping of gel self-assembly. RSC Advances. 2021;11(18):10710–26.
[39] Kumar N, Dixit A, Bag DS. Synthesis of highly swellable silver nanocomposite ionic double network (Ag-IDN) hydrogels and study of their characteristic properties. Polymer Bulletin. 2021 Aug 2;79(8):6759–76.

[40] Bardajee GR, Dianatnejad N, Mahmoodi NO, Mahmoodain H. Mechanical properties and development of silver Nanoparticle-enhanced Alginate-polyacrylamide double network Hydrogel. Journal of Polymer Research. 2024 Nov;31(11).
[41] Anselme K. Osteoblast adhesion on biomaterials. Biomaterials. 2000 Apr;21(7):667–81.
[42] Pasaribu SP, Ginting M, Masmur I, Kaban J, Hestina. Silver chloride nanoparticles embedded in self-healing hydrogels with biocompatible and antibacterial properties. Journal of Molecular Liquids. 2020 Jul;310:113263.
[43] Iqbal Y, Amin F, Usman Y, Farrukh Sarfraz M. Alginate-Based hydrogels with inorganic Nanomaterials: A promising approach for wound healing and bone tissue regeneration. European Polymer Journal. 2024 May;212:113057.
[44] Shumbula NP, Nkabinde SS, Ndala ZB, Mpelane S, Shumbula MP, Mdluli PS, et al. Evaluating the antimicrobial activity and cytotoxicity of polydopamine capped silver and silver/polydopamine core-shell nanocomposites. Arabian Journal of Chemistry. 2022 Jun;15(6):103798.
[45] Diniz F, Maia R, de Andrade LR, Andrade L, Vinicius Chaud M, da Silva C, et al. Silver Nanoparticles-Composing Alginate/Gelatine Hydrogel Improves Wound Healing In Vivo. Nanomaterials. 2020 Feb 23;10(2):390.